Patterning the second-order optical nonlinearity of asymmetric quantum wells by ion implantation enhanced intermixing

Patterning the second-order optical nonlinearity of asymmetric quantum wells by ion implantation enhanced intermixing

S. Janz,[a] M. Buchanan, P. van der Meer, Z. R. Wasilewski, and D.-X. Xu
Institute for Microstructural Sciences, National Research Council, Ottawa, Ontario, K1A 0R6, Canada

P. Piva, I. V. Mitchell, and U. G. Akano
Department of Physics, University of Western Ontario, London, Ontario, N6A 3K7, Canada

A. Fiore
Department of Electrical and Computer Engineering, University of California, Santa Barbara, California 93106-9560

(Received 10 February 1998; accepted for publication 10 April 1998)

The change in the second-order nonlinear susceptibility of an asymmetric quantum well (AQW) superlattice induced by ion beam-enhanced intermixing has been measured. The surface-emitted second-harmonic intensities radiated from implanted and masked areas of an AQW waveguide were measured and compared for incident wavelengths between $\lambda = 1480$ and 1600 nm. Intermixing resulted in a 60 meV blueshift of the AQW band edge and a uniform suppression of the AQW second-order susceptibility, while the masked AQWs were unchanged. © *1998 American Institute of Physics.* [S0003-6951(98)00324-6]

Wavelength translation by difference frequency generation (DFG) in a nonlinear waveguide has a number of advantages over other techniques, such as absolute transparency and little deterioration of the signal-to-noise ratio.[1] However, it is necessary to use quasi-phase matching (QPM) in a copropagating waveguide geometry to obtain conversion efficiencies sufficient for application in wavelength division multiplexed (WDM) networks. In QPM devices, a grating of alternating regions of high and low second-order susceptibility, $\chi^{(2)}$, is used to compensate the phase mismatch between the pump and signal beams. The local modification of the asymmetric quantum wells (AQW) by patterned intermixing can provide a method for implementing QPM in a semiconductor waveguide. For example, wavelength conversion could be achieved by mixing TE (transverse electric) mode pump light with a copropagating TM (transverse magnetic) mode signal beam in a waveguide containing a AQW superlattice, to produce a copropagating wavelength shifted TE signal beam at the difference frequency. QPM would be achieved by modulating $\chi^{(2)}$ of the AQWs periodically along the waveguide using a patterned ion implantation. Although the susceptibility modulation will be smaller[2–5] than that obtained by crystal domain QPM,[6] patterned quantum well intermixing uses a much simpler fabrication process. The magnitude of $\chi^{(2)}$ in an AQW superlattice[2–5] is comparable to that of many commonly used nonlinear crystals, and is easily modified using quantum well engineering techniques. Ion implantation enhanced quantum well intermixing is one such technique which has attracted much interest for post-growth fabrication of active and passive optical telecommunication components on a single wafer.[7–10] This letter presents measurements of the modulation in the second-order susceptibility at wavelengths between $\lambda = 1480$ and 1600 nm for a $GaAs/Al_xGa_{1-x}As$ AQW superlattice waveguide induced by patterned implantation enhanced intermixing.

Measuring the second-harmonic generation (SHG) response provides useful information for wavelength translation applications, since the susceptibility for SHG is similar to the susceptibility for DFG when the signal and difference frequencies are almost equal. For example, when the damping terms in the resonant denominators of the nonlinear susceptibilities can be neglected, the relation $\chi^{(2)}_{xzx}(2\omega+\Delta\omega, \omega\rightarrow\omega+\Delta\omega) \approx \chi^{(2)}_{xzx}{}^{*}(\omega, \omega+\Delta\omega\rightarrow 2\omega+\Delta\omega)$ holds between the dominant[2,3] AQW susceptibility components for sum-frequency generation and difference frequency generation.[11] In WDM applications, the frequency shift $\Delta\omega$ is very small and the sum frequency susceptibility is similar to the SH susceptibility measured in this experiment. As described in our previous work,[5] we use a unique surface emitting QPM waveguide geometry to separate the SHG response of the AQW superlattice from the larger bulk GaAs/AlGaAs response. In this work, an ion implantation mask is arranged to create intermixed and unchanged sections along a single AQW waveguide ridge. We can therefore simultaneously measure the SHG response from both sections without introducing the uncertainties caused by variations in waveguide coupling and internal losses from one waveguide to another.

The waveguide was grown by molecular beam epitaxy on a (100) GaAs substrate. A 0.6726 μm AQW superlattice is embedded between a 2 μm thick $Al_{0.5}Ga_{0.5}As$ lower cladding and a 0.6 μm thick $Al_{0.5}Ga_{0.5}As$ upper cladding. Each AQW is a coupled quantum well pair consisting of a 15 Å GaAs well separated from a 27 Å GaAs well by a 12 Å $Al_{0.4}Ga_{0.6}As$ barrier. These AQWs are separated from each other by a 160 Å $Al_{0.4}Ga_{0.6}As$ layer. The AQW superlattice is divided into six domains made up of five AQWs each. The orientation of the AQWs in each domain is reversed relative to the orientation in the adjacent domains. As a result the AQW contribution to $\chi^{(2)}$ in adjacent domains has opposite

[a]Electronic mail: siegfried.janz@nrc.ca

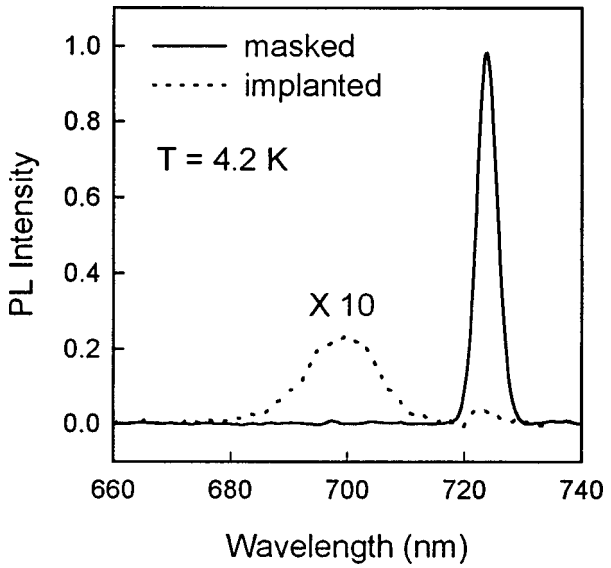

FIG. 1. Photoluminescence spectra at $T=4.2$ K for the masked and implanted areas of the asymmetric quantum well waveguide.

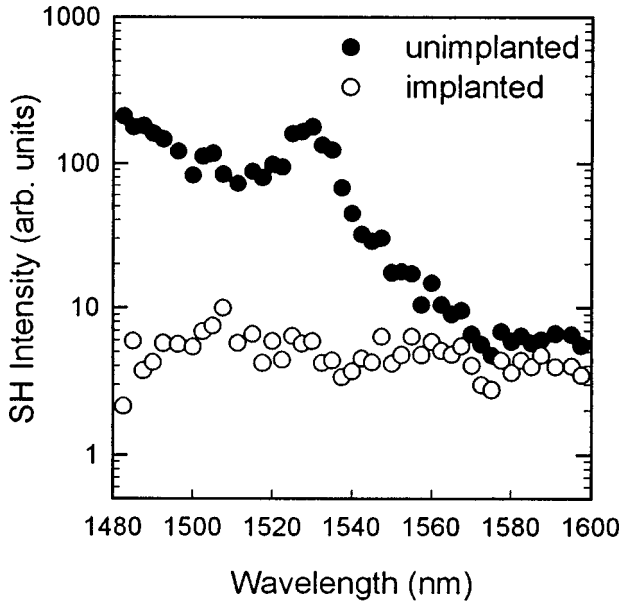

FIG. 2. Measured SH intensity spectra for the implanted and unimplanted regions of the AQW waveguide, for incident wavelengths between $\lambda=1480$ and 1600 nm.

sign. The 0.2232 μm period of the superlattice domain structure was chosen to quasi-phase match the AQW second-harmonic light radiated in the surface normal direction when pumped by counter-propagating waveguide modes near $\lambda=1550$ nm.

Waveguide ridges with widths between 4 and 10 μm were defined by wet etching. The wafer was then covered by a 100 nm plasma enhanced chemical vapor deposition (PECVD) oxide deposited at 250 °C, and a 1.5 μm thick Au implantation mask with rectangular openings to define 500 μm wide implanted and unimplanted strips running orthogonal to the waveguide ridges. The oxide layer prevents interaction of the Au and $Al_xGa_{1-x}As$ layers during implantation. The wafer was implanted using 5 MeV As^+ ions at a dose of 1×10^{13} ions cm^{-2} and at a temperature of 200 °C. TRIM[12] simulations of ion range and damage distributions were used to choose the ion energy and requisite Au mask layer thickness. End-of-range damage is more difficult to anneal than the vacancies and interstitials generated along an ion track[8,13] and can cause a serious deterioration of the quantum well optical properties.[8] The 5 MeV ion energy ensured that the end-of-range damage was located at a depth larger than 1.2 μm, well beyond the bottom of the AQW superlattice. A 1.5 μm thick Au implantation mask layer was required to prevent the 5 MeV As^+ ions from penetrating through to the underlying waveguide. After implantation the Au mask and oxide layers were stripped off, and the waveguide was annealed at 850 °C for 90 s. The annealing step removed implant damage and initiated quantum well interdiffusion in the irradiated AQW material.

Photoluminescence (PL) measurements were carried out at $T=4.2$ K using a $\lambda=632.8$ nm He-Ne laser as the excitation source. The PL spectra were collected before and after annealing from both the masked and unmasked areas. Figure 1 shows the PL spectra collected after annealing. In the unimplanted areas the AQW *e1-hh1* PL peak was located at $\lambda=724$ nm (1.713 eV) and remained unchanged in width and wavelength after annealing. We therefore conclude that annealing did not change the structure of the masked AQW superlattice. After annealing, a new PL peak is observed from the implanted regions at $\lambda=699$ nm (1.773 eV), indicating that the AQW *e1-hh1* transition had been blueshifted by 25 nm (60 meV). The width of this PL peak is also about four times greater (FWHM$\sim$28 meV) than from the unimplanted superlattice. Furthermore, the integrated PL intensity is reduced by an order of magnitude, suggesting that the intermixing process has reduced the nonradiative lifetime of the carriers in the AQWs. The observed broadening of the PL peak may arise from a number of contributions including interface roughening, increased alloy broadening as the wave functions penetrate further into the ternary barrier layers, as well as the variation in the degree of intermixing with depth.

The nonlinear response of the AQWs at room temperature was measured using an OH:NaCl color center laser, tunable between $\lambda=1480$ and 1610 nm. The 700 μm long AQW waveguide contained both intermixed and unimplanted regions along its length. The beam was coupled into the waveguide using a 40$\times$ microscope objective lens. A counterpropagating beam was provided by the reflection of the input beam from the end facet of the waveguide. The interaction of counterpropagating TE and TM components of the pump light[5,14] generates SHG light that is radiated along the surface normal. This surface-emitted SHG (SESHG) light was imaged onto a cooled CCD array positioned above the waveguide. At $\lambda=1528$ nm, the SH photon energy is near the AQW exciton resonance. The peak SH intensity radiated from the unimplanted section of the ridge is more than an order of magnitude larger than the SH radiated from the intermixed section. On the other hand, at $\lambda=1580$ nm the SESHG intensities emitted from the intermixed and unimplanted sections of the ridge are similar. The SH intensity spectra from the intermixed and unimplanted sections of the AQW ridge waveguide are shown in Fig. 2 for wavelengths between $\lambda=1480$ and 1600 nm. The SH spectrum from the unimplanted section is similar to that measured previously for the as grown waveguide,[5] except for a slight reduction of

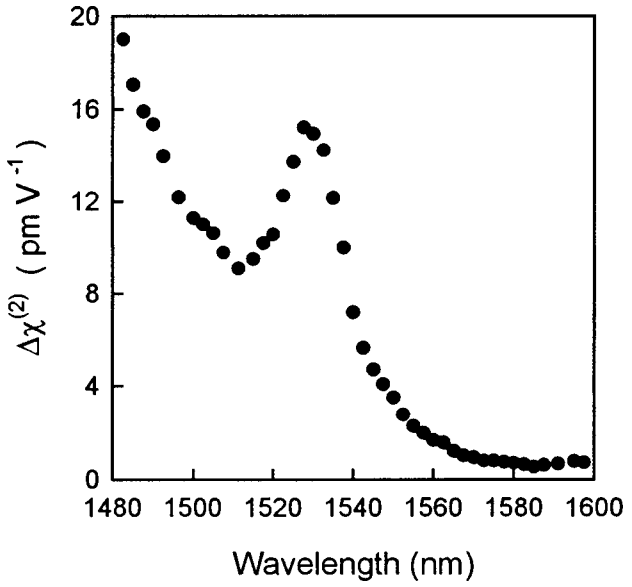

FIG. 3. The difference in the effective SH susceptibility, $\Delta\chi^{(2)}$, between the implanted and unimplanted AQW superlattices as derived from the data in Fig. 2.

the SH exciton resonance relative to the interband background signal. This may be due to a low but finite concentration of nonradiative defects introduced during fabrication. Note that at room temperature the exciton resonance is at $\lambda = 765$ nm for the unimplanted quantum wells. The SHG intensity spectrum for the intermixed AQWs is featureless and is much smaller than the intensity from the unimplanted AQWs at SH photon energies near and above the band gap.

In the surface-emitting QPM geometry, the radiating component of the quantum well SH polarization is proportional to an effective susceptibility given by the sum $\chi^{(2)} = \chi^{(2)}_{xzx} + \chi^{(2)}_{xyz}$, which is just the $\chi^{(2)}_{15}$ tensor element in the coordinate system rotated by 45° about the z axis.[15] The magnitude of $\chi^{(2)}$ has been measured to be approximately 20 pm V^{-1} at the exciton peak for the as grown superlattice.[5] The key parameter for designing intermixed QPM waveguides is the SH susceptibility difference $\Delta\chi^{(2)}$ between unimplanted and intermixed AQWs. Since the surface-emitting QPM resonance line shape is flat over the wavelength range in Fig. 2,[5] the SH intensities are approximately proportional to $|\chi^{(2)}|^2$. The data in Fig. 2 can therefore be used to determine the $\Delta\chi^{(2)}$ spectrum presented in Fig. 3.

Several effects contribute to the change in the SH susceptibility of the AQW superlattice after intermixing. The 60 meV blueshift of the band edge should displace the SH spectrum in Fig. 2 towards the blue by 50 nm, but leave the spectral features unchanged. The second effect is the broadening of the exciton resonance by inhomogeneous mechanisms such as the variation in intermixed quantum well width, as observed in the PL spectra of Fig. 1. At room temperature, the higher defect concentration in the implanted material may cause homogeneous lifetime broadening to become significant as well. However, the blueshifted interband contribution to the SH susceptibility should still be present. Finally, the quantum well SH susceptibility is nonzero only if the wells are asymmetric (i.e., they do not have inversion symmetry). The absence of any wavelength dependent features in the implanted SH spectrum in Fig. 2 suggests that the change in well shape (i.e., a decrease in asymmetry) does make a significant contribution to the suppression of the SH susceptibility.

To be useful for quasi-phase matching either SH generation $(\omega, \omega \rightarrow 2\omega)$ or wavelength (frequency) conversion by DFG $(2\omega + \Delta\omega, \omega \rightarrow \omega + \Delta\omega)$ devices, the AQW superlattice must be transparent to both the pump and output wavelengths. Therefore, only the intermixing induced modulation of $\chi^{(2)}$ for SH photon energies (or pump photon energies in the case of DFG wavelength conversion) below the band gap are useful. From Fig. 3, the region below the gap where $\Delta\chi^{(2)}$ is at least several pm V^{-1} extends from 1535 nm to approximately 1560 nm. Although this band is useful for WDM wavelength translation, it is clear that wavelength converters employing an AQW superlattice of the form described here will need to be tailored for specific and relatively narrow wavelength ranges.

In summary, we have measured the change in the SH susceptibility of an AQW superlattice induced by ion implantation enhanced intermixing. The $\chi^{(2)}$ of the unimplanted areas of our AQW waveguide remains unchanged after rapid thermal annealing, while the implanted areas show a uniform suppression of the SH response over the wavelength range between $\lambda = 1480$ and 1600 nm. The SH response is reduced by a combination of effects including a 60 meV blueshift of the AQW band edge, a broadening of the exciton resonance, and a reduction of the well asymmetry. The SH spectra indicate that there is a region approximately 25 nm wide at wavelengths just below the band edge which would be suitable for QPM wavelength conversion or SH generation.

[1] S. J. B. Yoo, J. Lightwave Technol. **14**, 955 (1996).
[2] J. Khurgin, J. Appl. Phys. **64**, 5026 (1988).
[3] A. Fiore, E. Rosencher, B. Vinter, D. Weill, and V. Berger, Phys. Rev. B **51**, 13192 (1995).
[4] S. Janz, F. Chatenoud, and R. Normandin, Opt. Lett. **19**, 622 (1994).
[5] A. Fiore, Y. Beaulieu, S. Janz, J. P. McCaffrey, Z. R. Wasilewski, and D. X. Xu, Appl. Phys. Lett. **70**, 2655 (1997).
[6] S. J. B. Yoo, C. Caneau, R. Bhat, and M. A. Khoza, Appl. Phys. Lett. **68**, 2609 (1996).
[7] S. Charbonneau, P. J. Poole, P. G. Piva, G. C. Aers, E. S. Koteles, M. Fallahi, J.-J. He, J. P. McCaffrey, M. Buchanan, M. Dion, R. D. Goldberg, and I. V. Mitchell, J. Appl. Phys. **78**, 3697 (1995).
[8] P. J. Poole, S. Charbonneau, G. C. Aers, T. E. Jackman, M. Buchanan, M. Dion, R. D. Goldberg, and I. V. Mitchell, J. Appl. Phys. **78**, 2367 (1995).
[9] P. J. Poole, S. Charbonneau, M. Dion, G. C. Aers, M. Buchanan, R. D. Goldberg, and I. V. Mitchell, IEEE Photonics Technol. Lett. **8**, 16 (1996).
[10] H. H. Tan, J. S. Williams, C. Jagadish, P. T. Burke, and M. Gal, Appl. Phys. Lett. **68**, 2401 (1996).
[11] Y. R. Shen, The Principles of Nonlinear Optics (Wiley, New York, 1984).
[12] J. F. Ziegler, Transport of Ions in Matter (TRIM), version 92.05 (IBM Research, Yorktown, New York, 1992).
[13] Y. B. Trudeau, G. E. Kajrys, G. Gagnon, and J. L. Brebner, Nucl. Instrum. Methods Phys. Res. B **59/60**, 609 (1991).
[14] R. Normandin, S. Létourneau, F. Chatenoud, and R. L. Williams, IEEE J. Quantum Electron. **27**, 1520 (1991).
[15] J. E. Sipe, D. J. Moss, and H. M. van Driel, Phys. Rev. B **35**, 1129 (1987).